NAVAL POSTGRADUATE SCHOOL

MONTEREY, CALIFORNIA

THESIS

PHASED ARRAY EXCITATIONS FOR EFFICIENT NEAR-FIELD WIRELESS POWER TRANSMISSION

by

Sean X. Hong

September 2016

Thesis Advisor: David Jenn
Second Reader: Roberto Cristi

Approved for public release. Distribution is unlimited.

THIS PAGE INTENTIONALLY LEFT BLANK

REPORT DOCUMENTATION PAGE			*Form Approved OMB No. 0704-0188*

1. AGENCY USE ONLY *(Leave blank)*	**2. REPORT DATE** September 2016	**3. REPORT TYPE AND DATES COVERED** Master's thesis

4. TITLE AND SUBTITLE
PHASED ARRAY EXCITATIONS FOR EFFICIENT NEAR-FIELD WIRELESS POWER TRANSMISSION

5. FUNDING NUMBERS

6. AUTHOR(S) Sean X. Hong

7. PERFORMING ORGANIZATION NAME(S) AND ADDRESS(ES)
Naval Postgraduate School
Monterey, CA 93943-5000

8. PERFORMING ORGANIZATION REPORT NUMBER

9. SPONSORING /MONITORING AGENCY NAME(S) AND ADDRESS(ES)
N/A

10. SPONSORING / MONITORING AGENCY REPORT NUMBER

11. SUPPLEMENTARY NOTES The views expressed in this thesis are those of the author and do not reflect the official policy or position of the Department of Defense or the U.S. Government. IRB Protocol number ____N/A____.

12a. DISTRIBUTION / AVAILABILITY STATEMENT
Approved for public release. Distribution is unlimited.

12b. DISTRIBUTION CODE

13. ABSTRACT (maximum 200 words)

This thesis is a continuation of an NPS project relating to the improvement of wireless-power transfer (WPT) in the near field. Improvement to power reception in the near field requires that excitation correction methods be applied to the transmitter antenna. The emphasis of this thesis is a parametric study of two correction methods to focus the transmitter array beam to the receiver array.

Quadratic-phase correction and complex-conjugate matching methods were investigated using Matlab and Savant to implement a simulation. Array size, frequency of operation, and distance between arrays were parameters used to gauge the improvement of power reception. Both methods demonstrated improvement over the uniform case at certain distances in the near field, with the complex-conjugate matching method proving to be the better option at very close ranges. Analysis and discussions of the advantages and disadvantages of each method are presented.

14. SUBJECT TERMS wireless power transmission, Matlab, Savant, near field, phase correction			**15. NUMBER OF PAGES** 65
			16. PRICE CODE
17. SECURITY CLASSIFICATION OF REPORT Unclassified	**18. SECURITY CLASSIFICATION OF THIS PAGE** Unclassified	**19. SECURITY CLASSIFICATION OF ABSTRACT** Unclassified	**20. LIMITATION OF ABSTRACT** UU

NSN 7540-01-280-5500 Standard Form 298 (Rev. 2-89)
Prescribed by ANSI Std. 239-18

THIS PAGE INTENTIONALLY LEFT BLANK

Approved for public release. Distribution is unlimited.

PHASED ARRAY EXCITATIONS FOR EFFICIENT NEAR-FIELD WIRELESS POWER TRANSMISSION

Sean X. Hong
Civilian, Department of the Navy
B.S., California Polytechnic State University, 2003

Submitted in partial fulfillment of the
requirements for the degree of

MASTER OF SCIENCE IN ELECTRICAL ENGINEERING

from the

NAVAL POSTGRADUATE SCHOOL
September 2016

Approved by: Dr. David Jenn
Thesis Advisor

Dr. Roberto Cristi
Second Reader

Dr. R. Clark Roberston
Chair, Department of Electrical and Computer Engineering

THIS PAGE INTENTIONALLY LEFT BLANK

ABSTRACT

This thesis is a continuation of an NPS project relating to the improvement of wireless-power transfer (WPT) in the near field. Improvement to power reception in the near field requires that excitation correction methods be applied to the transmitter antenna. The emphasis of this thesis is a parametric study of two correction methods to focus the transmitter array beam to the receiver array.

Quadratic-phase correction and complex-conjugate matching methods were investigated using Matlab and Savant to implement a simulation. Array size, frequency of operation, and distance between arrays were parameters used to gauge the improvement of power reception. Both methods demonstrated improvement over the uniform case at certain distances in the near field, with the complex-conjugate matching method proving to be the better option at very close ranges. Analysis and discussions of the advantages and disadvantages of each method are presented.

THIS PAGE INTENTIONALLY LEFT BLANK

TABLE OF CONTENTS

THIS PAGE INTENTIONALLY LEFT BLANK

LIST OF FIGURES

LIST OF ACRONYMS AND ABBREVIATIONS

API	application programming interface
CAD	computer-aided design
CEM	computational electromagnetic
CW	continuous wave
DC	direct current
GO	geometrical optics
HTML	hypertext markup language
ISM	Industrial, Scientific, and Medical
LOS	line-of-sight
MAV	micro unmanned aerial vehicle
PEC	perfect electrical conductor
PO	physical optics
RF	radio frequency
SBR	shooting and bouncing ray
TE	transverse electric
TEM	transverse electromagnetic
TM	transverse magnetic
UAV	unmanned aerial vehicles
VSWR	voltage standing wave ratio
WPT	wireless power transfer
XML	extensible markup language

THIS PAGE INTENTIONALLY LEFT BLANK

ACKNOWLEDGMENTS

I would like to thank Leana Kim, my wife, for her enduring patience and support. I also want to thank my kids for their understanding of why their father could not play with them for the hundredth time. Finally, I would like to thank Dr. Jenn for his guidance and help with crafting my thesis.

THIS PAGE INTENTIONALLY LEFT BLANK

I. INTRODUCTION

A. BACKGROUND

In 2015, as reported in the *Navy Times* [1], U.S. Navy Secretary Ray Mabus suggested that the F-35 Joint Strike Fighter "should be the last manned strike fighter aircraft the Department of Navy will ever buy or fly." What can be inferred from this statement is that unmanned aerial vehicles (UAVs) will continue replacing manned aircraft in essential missions and in support of ground forces to accomplish their missions. Although there are advantages and disadvantages to using UAVs, the belief that UAVs will eventually replace manned vehicles will fuel further improvements in UAV technology. One of these areas is the ability to charge the UAV systems without having to hardwire a connection to a power source. To achieve this, a microwave signal from a base station can be used to charge the UAV once it lands, as shown in Figure 1. Because of the close proximity of the UAV to the base station, the electromagnetic beam falls within the Fresnel region. This wireless power transmission (WPT) approach has been studied extensively in the past to implement this concept and maximize the transfer efficiency.

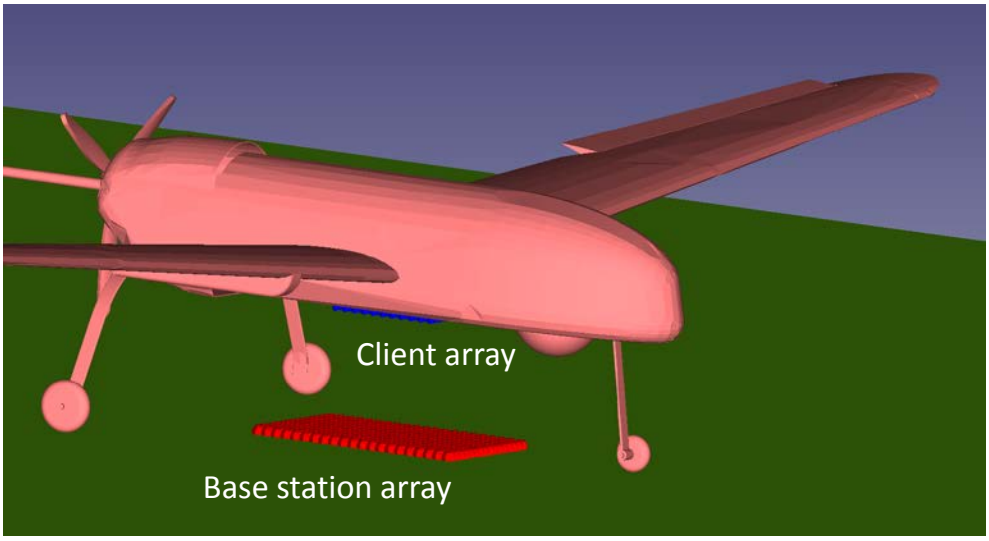

Figure 1. Concept Drawing of a Base Station Array Wirelessly Transferring Power to a Grounded UAV

Wireless power transfer has been explored and analyzed using both an inductive approach and a radiative approach [2]–[9]. In Figure 2, the block diagram for the WPT system is shown. The power station provides the power that is used to charge the power plant or battery in the client. The power starts off as low frequency A/C power, so conversion to radio frequency (RF) is needed to change the power to RF so that the signal can be transmitted via an antenna or coil. On the client side, the rectifying antenna receives the RF power, filters, and conditions the power (transforms its voltage and current to direct current (DC)) so that it can be channeled to the battery or power plant.

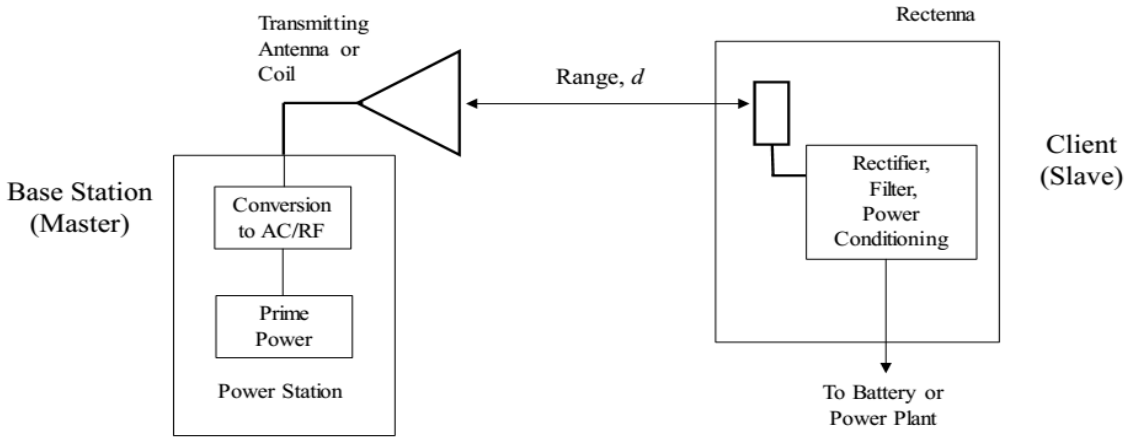

Figure 2. WPT System Block Diagram for Battery Charging. Source: [2].

Wireless power transfer has gained renewed interest since the advent of cell phone technology as well as increased drone usage in the military; although the interest has always been there, the minimization of circuit components, as well as the advent of increased processing power and memory size, permits the implementation of efficient WPT for commercial as well as military applications.

From a smartphone user's standpoint, down time for recharging a cell phone means the user has less time to conduct business, work on a project, or just leisurely play a game. From the mission standpoint, if the operator needs to recharge the drone, then this situation equates to one less asset to fulfill the mission. Any downtime can have dire consequences for ground forces that rely on the drones to be their eyes, to destroy a

critical enemy outpost, or to transport equipment. In other words, the longer the drone is up and running, the more we can support troops in the field.

The space surrounding an antenna can be broken down into three regions [10]: (1) reactive near field, (2) radiating near field, and (3) far field. From a distance of 0 to $0.62\sqrt{D^3/\lambda}$, where D is the largest dimension of the antenna and λ is the wavelength, the reactive near field dominates. From $0.62\sqrt{D^3/\lambda}$ to $2D^2/\lambda$, "the radiation fields predominate and its angular field distribution is dependent upon the distance from the antenna. The field pattern is, in general, a function of the radial distance and the radial field component may be appreciable" [10]. This region may not exist if the largest dimension of the antenna is minimal relative to the wavelength. This region is also commonly referred to as the Fresnel region. The region from $2D^2/\lambda$ to infinity is known as the far-field region. In this region, the radiation pattern is independent of distance [11]. In the near field, because of the dependency of the radiation pattern on the distance to the antenna, special techniques are required to maximize the power at a close distance to the antenna.

Technological limitations prevented earlier pioneers in the WPT realm from implementing efficient concepts. Since rectification is a nonlinear process, without precisely knowing the power level at a given distance from the antenna, it is very difficult to operate the rectenna (a special type of antenna that is used to convert electromagnetic energy into DC power at maximum efficiency. Lacking an efficient method for delivery, WPT is not practical. Today, technological advances enable processors to compute more quickly and begin to solve these efficiency issues. Commercial software, such as Savant, allows the user to simulate the radiated field distribution in the near-field environment of the antenna, allowing for an optimum rectenna design.

B. PREVIOUS WORK

Previous work has been done in the analysis of near-field focusing for WPT, specifically in [2]. The WPT method was introduced in the 1960s for vehicle propulsion, and researchers from Raytheon eventually developed and demonstrated the method [12].

With the successful demonstration, the next step was to improve the efficiency of the power delivered as well as the form factor for the system. Much of the recent research has been geared towards improving these two criteria in the near field, as an improvement in processing power has lent itself to improvements in the WPT performance.

In [3], Ling and Yoon surmised a new analytical upper bound for power transfer efficiency (PTE) for WPT using a pair of antennas separated by a spherical material shell and showed that lossy dielectric materials disturb the transverse magnetic (TM) and transverse electric (TE) mode radiators. Numerical simulation using *FEKO* validated the theoretical formulation, where *FEKO* is a German acronym for "FEldberechnung für Körper mit beliebiger Oberfläche" meaning "field calculations involving bodies of arbitrary shape."

Zhang and Cheng [13] experimented with two efficient, electrically small planar antennas and found that these two antennas could reach high PTE without adaptive matching methods.

In the commercial world of cell phones, laptops, tablets, etc., Li and Jandhyala [14] examined the use of a retrodirective antenna array for WPT with the antenna placed at a static location charging randomly placed devices within that room. They provided design guidelines using a lookup table for different parameters: element number, element size, spacing, and focus distance.

Other researchers such as Deng and Kong [4] focused their efforts on improving the components in the WPT system, more specifically the rectenna. Using a common diode they simulated the rectenna performance using their new method and theory that provided an output of 25.6 mW and 52% conversion efficiency; however, researchers in Japan [6] chose to develop new substrates in order to improve the RF-to-DC conversion efficiency. They demonstrated an RF-to-DC conversion efficiency of 74.4% at 2.45 GHz at a 5-W input power using a 10-finger GaN Schottky diode. Working on improving the form factor of the rectennas, researchers in Korea [15] designed a low-profile printed

rectenna in the X-band that showed a 7% and 4% maximum efficiency for a two-by-two array rectenna and a four-by-four rectenna, respectively.

The researchers from Sendai National College of Technology and Tohoku University [16] calculated the transfer efficiency of a WPT system by using the scattering parameters (S-parameters) of the WPT system modeled as a two-port lossy network. Using this general and practical method, they found that the maximum transfer efficiency occurred when the input and output ports are both conjugately matched.

On the same note, Koziel and Mongiardo [17] derived a surrogate-based optimization method for improving transfer efficiency using equivalent network theory and conjugate-image impedances. Although a full-wave optimization is ideal for practical cases, the researchers showed that the surrogate based optimization was a fair approximation.

With regard to the near field, work has been done to improve the transfer efficiency using several adaptive matching methods, specifically simultaneous conjugate matching, frequency tracking, and a combination of the two [18]. Because the simultaneous conjugate matching method was not practical and the frequency matching method showed poor performance beyond the strongly coupled region of the two antennas, the hybrid frequency tracking method with a complex load matched at the target distance proved to have stable efficiency across the near-field region.

At the Naval Postgraduate School, research in the area of WPT has gained momentum over the years. In 1998, Suksong [19] discovered that a monopole on a cylindrical end cap provided the lowest voltage standing wave ratio (VSWR) and a nearly hemispherical radiation pattern based on four different antenna configurations. He planned to use this antenna to remotely power a micro UAV (MAV) [19]. Continuing on the work of remotely powering the MAV, Vitale [20] studied several microwave rectifier systems and eventually achieved a maximum RF-to-DC conversion efficiency of 33%. He also showed that 1.8-W, 1.3 GHz microwave signal could power a miniature DC motor in free space at a distance of 30 inches from the transmitter antenna. In 2003, Tsolis [21] demonstrated that a MAV weighing between 9 and 15 grams and deriving the

components from previous research to work at a different frequency can be powered via WPT at 10 GHz. Further work was done by Tan [22] to improve on several subsystems (receiving antenna, pre-rectification filtering, rectifier, and post-rectification filter) of the MAV and reduce its dimensions and weight. He realized a final design with an overall dimension of 112.5 mm^2, an estimated weight of less than a gram, and an RF-to-DC conversion efficiency of 50%. Toh [23] built the 10 GHz microstrip rectenna suggested by previous research and accomplished a conversion efficiency of 26%-37% per rectenna element, a fourfold improvement over [21]. Adding to the work on improving rectenna design, Liu [24] found that a dipole antenna array used as full-wave rectenna without low-pass filter showed a conversion efficiency of 65% and also reduced the weight of the overall system. In 2012, Huang [25] investigated how best to optimize the full-wave rectenna and obtained a maximum efficiency of 57% at 10 GHz with a 200 mW input.

In the present research, we build on the previous work in [2] and examine several ideas to improve the efficiency in the near field for an array-to-array configuration.

C. OBJECTIVE AND APPROACH

In [2], a digital phased array is used on the transmit side to form a narrow beam to illuminate the client receive antenna. There are many caveats in order to optimize the efficiency in transferring power to the client antenna. First, when a receiving point is in the near-field of a transmitter antenna, the phase for each element in the array needs to be corrected to create a focused beam; however, the correction focusses the maximum at a point. If the receiver antenna has a large area, or is very close to the transmitter antenna, then some of the receiver elements will be outside of the transmitter beam. Analysis of the client antenna must determine amplitude and phase corrections required to address this issue so that more of the client antenna's surface area can be coherently illuminated by the focused beam to ensure more power can be transferred.

One proposed solution to address the phase error problem is to divide the transmitter array into subarrays to create multiple beams that can be individually focused to cover more of the client antenna aperture. Creating the correct excitations to synthesize each subarray beam is a challenge to efficient operation. Amplitude and phase corrections

on the client antenna for each subarray beam need to be applied so that all beams are combined coherently. All these requirements can be simulated using Matlab and verified using Savant (a commercial antenna modelling software).

In this thesis, we are concerned with the radiative approach to the charging problem based on the operating range (distance) of interest. Typically, when the client is charging, the distance from the charging base station is not more than 3.0 m, so the far-field condition may not be satisfied. If the transmitter array uses uniform amplitude and phase weighting across its elements, the full gain of the antennas is not achieved in the near field. The spherical phase error correction method (also referred to as a quadratic-phase correction) serves to solve the near-field issue of unfocused energy in the Fresnel zone. In Figure 3, a typical case where the focused array achieves a 12 dB improvement over the unfocused array at distances less than 3.0 m for a transmitter array with a single receiver dipole at 300 MHz is shown. In this thesis, we expand the radiative approach beyond a single receiver dipole by considering various transmitter and receiver array sizes. Along with the quadratic-focusing method, we also explore the focused complex-conjugate matched method. The complex-conjugate method calculates the transmitted field at the points where the receiver antenna elements are located, and then conjugate field weights are applied to the transmitter antenna elements.

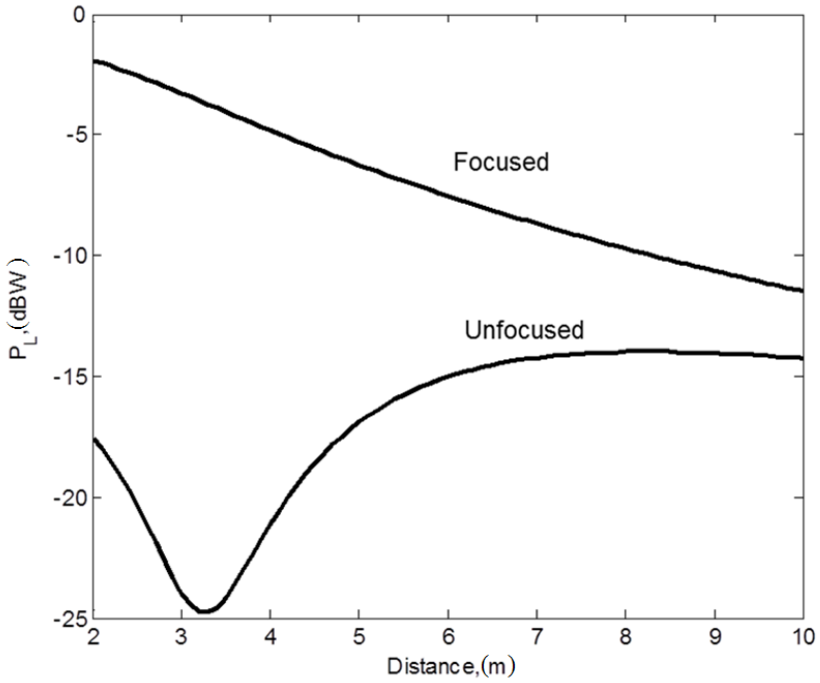

Figure 3. Savant Simulations for Near-Field Ranges with and without Quadratic Focusing. The Scenario is Power Received by a Single Dipole with a Matched Load over a Ground Plane from a Ten-by-Ten Array with Ground Plane Transmitting 1.0 W at 300 MHz. Source: [2].

The approach to achieving these comparisons is first to develop an analytical model for the antenna transmission so that parametric dependencies are established. After creating the model, we employ simulations using computational electromagnetic (CEM) software to conduct the parametric studies and determine the most efficient, or optimum, configuration and operating conditions.

The following parameters are varied: operating frequency, distance between the transmitter and receiver arrays, and sizes of the transmitter and receiver arrays. Several operating frequencies are considered to examine how the spherical phase-error correction method affects the overall power received by the UAV. Using the same dimensions and extending the error correction to include conjugate matching, we show the advantages of using conjugate matching over a simple phase-error correction. Finally, tradeoffs are discussed between the two methods to determine the best overall method for WPT.

D. THESIS OUTLINE

In Chapter II, an analytical model and its equations are developed that lay the foundation for simulations. The spherical error correction is discussed, as well as the conjugate matched correction.

In Chapter III, we present the approach to the parametric study, a Savant software overview, including its advantages and limitations, and the simulation process and programming required to automate the parametric study. The simulation results for the unfocussed, quadratic correction and conjugate matched cases are discussed.

In Chapter IV, the results are summarized, and a conclusion for the study is provided. Future areas of research that were not included in this study are suggested.

THIS PAGE INTENTIONALLY LEFT BLANK

II. ANALYSIS

A. MODEL

1. System Design

Within the WPT system, the master station transmits a continuous wave (CW) to the client. For the master station, the antennas tend to be of the high gain variety, focusing continuously at the client. On the receiver end, the UAV antenna typically is low gain and small in size because of platform limitations. The received power versus system parameters are governed by the Friis equation [26]

$$P_r = \frac{P_t G_t G_r \lambda^2 L}{(4\pi d)^2} |F|^2 \tag{1}$$

where P_t is the transmitted power, G_t is the charging station antenna gain, G_r is the receiver (client) antenna gain, and $\lambda = c/f$ is the wavelength (c is the speed of light, f is the frequency in Hz). The factor F accounts for wave propagation effects in the medium, such as multipath and attenuation, L is an efficiency factor that includes device losses, rectifier efficiency, and separation d is the center-to-center spacing between the antennas.

In the far field, the antenna gains G_t and G_r are given by the general formula [26]

$$G = \frac{4\pi A_e}{\lambda^2} \tag{2}$$

where A_e is effective area.

2. Near Field Formulation

a. Transmitter Array

Typically, when the UAV is charging, the receiver antenna on the UAV and the transmitter antenna on the charging station are in each other's near field. If no adjustments are made to the antennas and uniform amplitude and phase weighting is utilized, then the full gain of the antennas is not realized. With full control of the array

elements' amplitude and phase, the charging station may utilize near-field focusing. Each element can be fed by a transmit module that is controlled by the digital beamforming processor. The processor calculates the phase difference between each transmitter array element and the receiver array element and, thereby, calculates the amplitude and phase weight for each transmit module. By doing so, the transmitter array focuses more of its energy on the receiver array [2].

In Figure 4, the near-field geometry is shown. For a general case, let the array focal point be at $\overrightarrow{r_f}\left(x_f, y_f, z_f\right)$ and the observation (field point) be at $\vec{R}(x, y, z)$. The array is located in the *x*-*z* plane and has a rectangular grid with N_x by N_z elements ($1 \le m \le N_x$ and $1 \le n \le N_z$) spaced d_x by d_z, respectively [2]. The normal vector to the array is $\hat{y}$.

The other parameters that are shown in Figure 4, as described in [2], are the position vector to element m,n, $\vec{d}_{mn} = x_{mn}\hat{x} + z_{mn}\hat{z}$, where

$$x_{mn} = \frac{2m - \left(N_x + 1\right)}{2} d_x, \tag{3}$$

$$z_{mn} = \frac{2n - \left(N_z + 1\right)}{2} d_z, \tag{4}$$

and

$$y_{mn} = 0. \tag{5}$$

The position vector to the focal point is given by

$$\overrightarrow{r_f} = x_f\hat{x} + y_f\hat{y} + z_f\hat{z}, \tag{6}$$

and the position vector to the field point is

$$\vec{R} = x\hat{x} + y\hat{y} + z\hat{z}. \tag{7}$$

The vector from element *m, n* to the focal point is

$$\vec{R}_{mn} = \left(x_f - x_{mn}\right)\hat{x} + \left(y_f - y_{mn}\right)\hat{y} + \left(z_f - z_{mn}\right)\hat{z}\,, \tag{8}$$

and the vector from element *m, n* to the field point is

$$\vec{r}_{mn} = \left(x - x_{mn}\right)\hat{x} + \left(y - y_{mn}\right)\hat{y} + \left(z - z_{mn}\right)\hat{z}\,, \tag{9}$$

where

$$\hat{r}_{mn} = \frac{\vec{r}_{mn}}{\left|\vec{r}_{mn}\right|}. \tag{10}$$

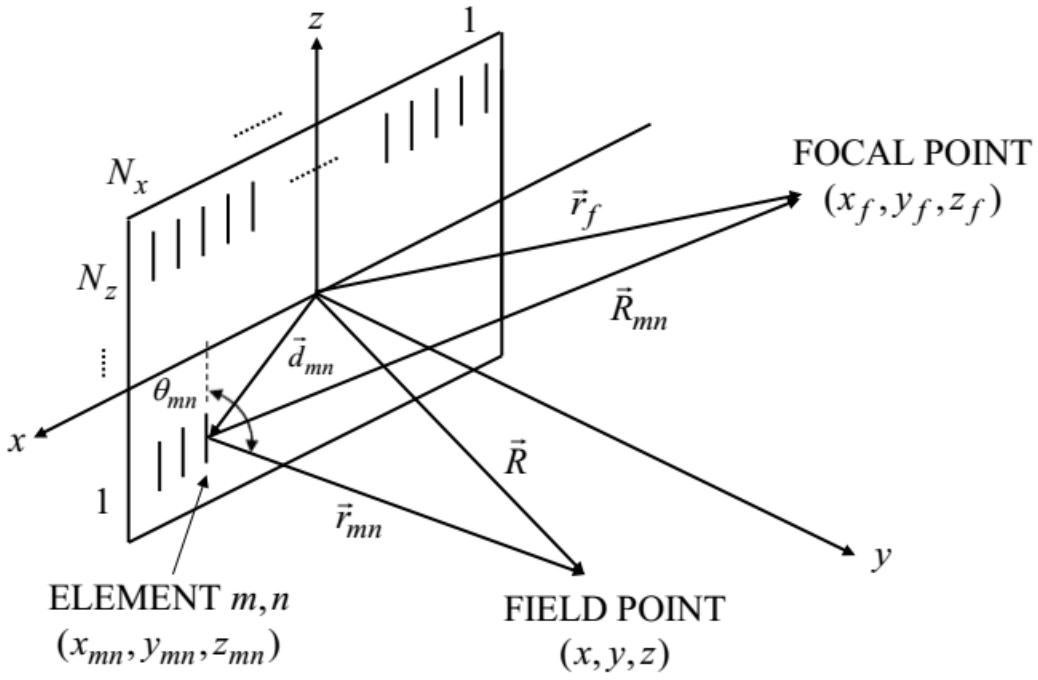

Figure 4. Planar Array Antenna Near-Field Model. Source: [2].

Let the elements be z-directed and linearly polarized. A general form for the element factor is [2]

$$\vec{F}_{mn}\left(\theta_{mn},\phi_{mn}\right)=\hat{z}C_o\Psi\left(r_{mn}\right)f_{mn}\left(\theta_{mn},\phi_{mn}\right) \tag{11}$$

where $f_{mn}\left(\theta_{mn},\phi_{mn}\right)$ is the normalized element pattern as a function of angles θ_{mn},ϕ_{mn}, $\Psi\left(r_{mn}\right)=e^{-j\beta r_{mn}}/r_{mn}$ is the free space Green's function with $\beta=2\pi/\lambda$, C_o a complex constant that depends on the element type (e.g., dipole, patch, etc.), θ_{mn} is the angle between the element m,n axis (along the z-axis) and the field point position vector

$$\cos\theta_{mn}=\hat{z}\cdot\hat{r}_{mn},\sin\theta_{mn}=\sqrt{1-\cos^2\theta_{mn}}\,, \tag{12}$$

and ϕ_{mn} is the element azimuth angle where

$$\tan\phi_{mn}=\frac{y_f-y_{mn}}{x_f-x_{mn}}. \tag{13}$$

Normally, all elements of an array are the same, exhibiting the relationships $\vec{F}_{mn}\left(\theta_{mn},\phi_{mn}\right)\equiv\vec{F}\left(\theta_{mn},\phi_{mn}\right)$ and $f_{mn}\left(\theta_{mn},\phi_{mn}\right)\equiv f\left(\theta_{mn},\phi_{mn}\right)$. If the elements are unit current amplitude, z-directed half-wave dipoles at height h above a ground plane that is a perfect electrical conductor (PEC), then the element factor is [2]

$$\vec{F}\left(\theta_{mn},\phi_{mn}\right)=j120\hat{z}\underbrace{\frac{e^{-j\beta r_{mn}}}{r_{mn}}}_{\Psi(r_{mn})}\underbrace{\frac{\cos\left(\frac{\pi}{2}\cos\theta_{mn}\right)}{\sin\theta_{mn}}\sin\left(\beta h\sin\theta_{mn}\sin\phi_{mn}\right)}_{f(\theta_{mn},\phi_{mn})}. \tag{14}$$

The ground plane factor (the last sine factor in Eq. (14)) is for a distance in the far field of the element. This factor is only relevant for the idealized case of an "isolated element above an infinite ground plane. The ground plane factor for a dipole over a finite ground plane, in an array environment, or in the near field will differ from $\sin\left(\beta h\sin\theta_{mn}\sin\phi_{mn}\right)$ due to mutual coupling and diffraction" [2].

The total array field at the observation point is given by the weighted sum

$$\begin{aligned}\vec{E}(R,\theta,\phi) &= \sum_{m=1}^{N_x}\sum_{n=1}^{N_z} A_{mn} e^{j\Phi_{mn}} e^{j\psi_{mn}} \vec{F}(\theta_{mn},\phi_{mn}) \\ &= j120\hat{z}\sum_{m=1}^{N_x}\sum_{n=1}^{N_z}\left\{\frac{e^{-j\beta r_{mn}}}{r_{mn}} f(\theta_{mn},\phi_{mn}) A_{mn} e^{j\Phi_{mn}} e^{j\psi_{mn}}\right\}\end{aligned} \tag{15}$$

where A_{mn} is the element's current amplitude coefficient, Φ_{mn} is the phase required to focus the beam at r_f, $\Phi_{mn} = \beta\left(r_f - r_{mn}\right)$, and ψ_{mn} is a miscellaneous calibration and correction phase.

We exploit these relationships at the transmitter as well as the receiver to improve the received power. Next we describe the combination of signals at the receiver.

b. Receiver Array

Let a receiver array be centered on the y-axis at y_{p_o} with numbers of elements in the *x* and *z* directions N'_x and N'_z and spacings d'_x and d'_z, respectively [2]. Similar to the transmitter array, the element locations are given by $x'_{pq} = \left[2p - \left(N'_x + 1\right)d'_x\right]/2$, $z'_{pq} = \left[2q - \left(N'_z + 1\right)d'_z\right]/2$ and $y'_{pq} = 0$ $\left(1 \le p \le N'_x, 1 \le q \le N'_z\right)$ as shown in Figure 5.

For the receiver array, we use primed quantities and indices to differentiate from the transmitter array quantities and indices. The incident field at element *p,q* is obtained by setting its location as the field point in Figure 4:

$$\vec{E}^i(R,\theta,\phi) \rightarrow \vec{E}^i\left(x'_{pq}, y'_{pq}, z'_{pq}\right) \equiv \vec{E}^i_{pq}. \tag{16}$$

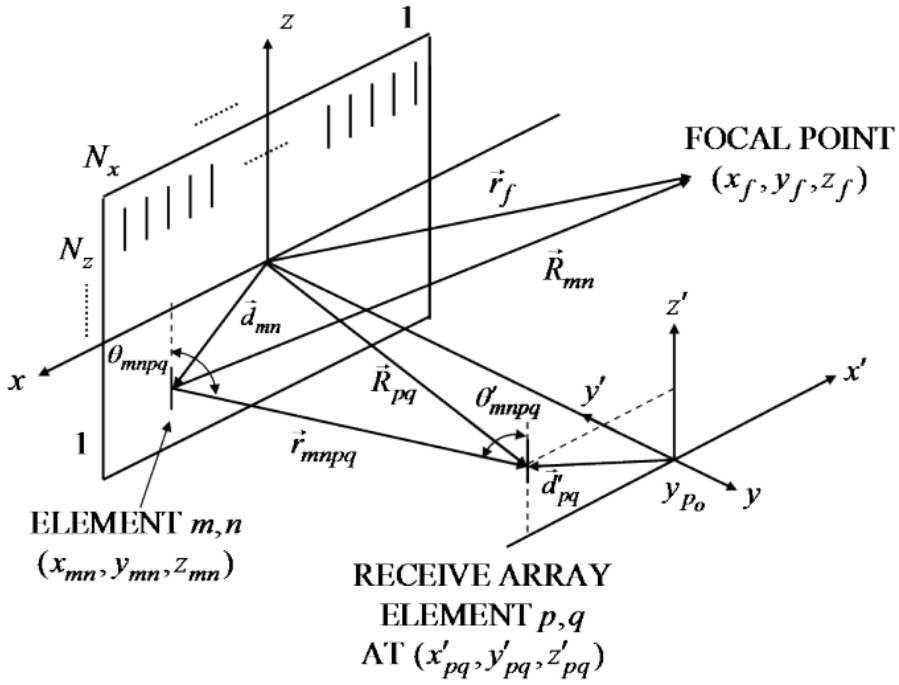

Figure 5. Total Field at Element p, q of the Receiver Array. Source: [2].

Inserting the appropriate values into Eq. (15), the total field at element *p,q* affected by the transmitter array elements is given by

$$\vec{E}^{i}_{pq} = j120\hat{z}\sum_{m=1}^{N_x}\sum_{n=1}^{N_y}\left\{\frac{e^{-j\beta r_{mnpq}}}{r_{mnpq}} f\left(\theta_{mnpq}, \phi_{mnpq}\right) A_{mn} e^{j\Phi_{mn}} e^{j\psi_{mn}}\right\} \tag{17}$$

where

$$\vec{r}_{mnpq} = \left(x_{pq} - x_{mn}\right)\hat{x} + \left(y_{pq} - y_{mn}\right)\hat{y} + \left(z_{pq} - z_{mn}\right)\hat{z}, \tag{18}$$

$r_{mnpq} = \left|\vec{r}_{mnpq}\right|$ and θ_{mnpq} is the angle of the axis of transmitter element m, n with the line of sight (LOS) vector to receive element *p,q* (an extension of Eq. (12)), and [2]

$$\cos\left(\theta_{mnpq}\right) = \frac{\vec{r}_{mnpq} \cdot \hat{z}}{\left|\vec{r}_{mnpq}\right|}. \tag{19}$$

By the same token and using Eq. (13), the azimuth angle is

$$\tan\left(\phi_{mnpq}\right)=\frac{y_{pq}-y_{mn}}{x_{pq}-x_{mn}}. \tag{20}$$

Receiver element *p, q* outputs a complex voltage given by

$$V_{pq}=\vec{E}^{i}_{pq}\cdot\vec{h}_{pq}\left(\theta'_{mnpq},\phi'_{mnpq}\right) \tag{21}$$

where $\vec{h}_{pq}$ is the effective height vector of receive element *p,q* and $\left(\theta'_{mnpq},\phi'_{mnpq}\right)$ is the direction from the receiver element axis with the LOS to transmitter element m, n with

$$\cos\left(\theta'_{mnpq}\right)=\frac{\vec{r}_{mnpq}\cdot\hat{z}'_{pq}}{\left|\vec{r}_{mnpq}\right|} \tag{22}$$

and

$$\tan\left(\phi'_{mnpq}\right)=\frac{y'_{mn}-y'_{pq}}{x'_{mn}-x'_{pq}}. \tag{23}$$

The relationship between the receiver and transmitter array is given by

$$\hat{z}'=\hat{z},\hat{x}'=-\hat{x},\hat{y}'=-\hat{y} \tag{24}$$

and each point is determined from

$$z'=z,x'=-x,y'=-y. \tag{25}$$

In the Appendix, the derivation of the effective height for a half-wave dipole on the z'-axis above a PEC ground is developed, and the result is

$$\vec{h}_{pq}=-j\frac{4}{\beta}f\left(\theta'_{mnpq},\phi'_{mnpq}\right)\hat{\theta}'. \tag{26}$$

This final form is “an idealized case of an isolated element above an infinite ground plane” [2]. For a “dipole over a finite ground plane or in an array environment,” [2] mutual coupling and diffraction alter the effective height. Finally, the “total complex voltage at the output of the receiving array” [2] can be calculated and determined to be the complex sum of all receiver dipole voltages

$$
\begin{aligned}
V_{out} &= \sum_{p=1}^{N_x'}\sum_{q=1}^{N_z'} V_{pq} A_{pq}' e^{j\psi_{pq}'} \\
&= j\frac{480}{\beta}\sum_{p=1}^{N_x'}\sum_{q=1}^{N_z'}\sum_{m=1}^{N_x}\sum_{n=1}^{N_y}\left\{\hat{z}\cdot\hat{\theta}_{pq}' h_{pq}\left(\theta_{mnpq}', \phi_{mnpq}'\right) A_{pq}' e^{j\psi_{pq}'}\right. \\
&\left.\times\Psi\left(r_{mnpq}\right) f\left(\theta_{mnpq}, \phi_{mnpq}\right) A_{mn} e^{j\Phi_{mn}} e^{j\psi_{mn}}\right\}
\end{aligned}
\tag{27}
$$

where A_{pq}' and ψ_{pq}' are miscellaneous calibration and correction amplitudes and phases applied at the receiver, and $\hat{\theta}_{pq}'$ is spherical system unit vector centered at *p,q*. Given that Eqs. (23) hold

$$
\hat{z}\cdot\hat{\theta}_{pq}' = -\sin\theta_{mnpq}'. \tag{28}
$$

"For both arrays with half-wave dipoles above a PEC ground plane," [2] the final result is

$$
\begin{aligned}
V_{out} = j\frac{480}{\beta}\sum_{p=1}^{N_x'}\sum_{q=1}^{N_z'} A_{pq}' e^{j\psi_{pq}'}\left\{\sum_{m=1}^{N_x}\sum_{n=1}^{N_y}\sin\theta_{mnpq}'\left(\frac{e^{-j\beta r_{mnpq}}}{r_{mnpq}}\right)\left[\frac{\cos\left(\frac{\pi}{2}w_{mnpq}\right)}{\sqrt{1-w_{mnpq}^2}}\sin\left(\beta h v_{mnpq}\right)\right]\right. \\
\left.\times A_{mn} e^{j\Phi_{mn}} e^{j\psi_{mn}}\left[\frac{\cos\left(\frac{\pi}{2}w_{mnpq}'\right)}{\sqrt{1-\left(w'\right)_{mnpq}^2}}\sin\left(\beta h v_{mnpq}'\right)\right]\right\}
\end{aligned}
\tag{29}
$$

where $v_{mnpq} = \sin\theta_{mnpq}\sin\phi_{mnpq}$, $w_{mnpq} = \cos\theta_{mnpq}, \sin\theta_{mnpq} = \sqrt{1-w_{mnpq}^2}$,

$v_{mnpq}' = \sin\theta_{mnpq}'\sin\phi_{mnpq}'$, and $w_{mnpq}' = \cos\theta_{mnpq}', \sin\theta_{mnpq}' = \sqrt{1-\left(w'\right)_{mnpq}^2}$.

As can be seen in Eq. (29), a summation of the elements' voltages is considered for series combination. In contrast, when the dipoles are arranged in a parallel combination, voltage remains constant and results in $V_{out}/\left(N_x'N_z'\right)$. The time-average power is

$$P_L = \frac{1}{2}\mathrm{Re}\left\{VI^*\right\} = \frac{1}{2\left(N_x' N'\right)}\mathrm{Re}\left\{V_{out} I_{out}^*\right\}. \tag{30}$$

The power delivered to a conjugate-matched receiver load of resistance R_L is [10]

$$P_L = \frac{\left|V_{out}\right|^2}{\left(N_x' N'\right) 8 R_L}. \tag{31}$$

3. Quadratic-Phase Error Assumption and Correction

If a point source with spherical wave fronts illuminates an aperture, as shown in Figure 6, then there is a path difference between the center of the aperture and the edge; therefore, this path difference results in a phase error $\beta\Delta = 2\pi\Delta/\lambda$. From Figure 6,

$$R^2 + x^2 = \left(R + \Delta\right)^2 \tag{32}$$

which gives

$$\Delta = R\sqrt{1 + \left(\frac{x}{R}\right)^2} - R. \tag{33}$$

Applying a Taylor expansion to Eq. (33), we get

$$\Delta = R\left(1 + \frac{1}{2}\left(\frac{x}{R}\right)^2 + \ldots\right) - R. \tag{34}$$

Keeping only the first two terms, we get a quadratic phase error of $\Delta\left(x\right) \approx x^2/2R$. Substituting the quadratic phase error into Eq. (15) gives $e^{-j\beta x^2/2R}$ as the phase term because the $R + \Delta$ path is longer than R; therefore, the quadratic-phase error correction needed is $e^{j\beta x^2/2R}$. Since the quadratic-phase error correction only requires knowledge of the receiver array's center, this method requires less processing than conjugate-field matching.

When the distance between the transmitter and receiver arrays is large (the far-field case), the spherical wave fronts are essentially plane waves, and the phase error is minimal across the array. As the distance is shortened between the two arrays, the phase error increases. The phase error correction holds as long as the transmitter array appears to be a point source; however, as the distance between the transmitter and receiver arrays shorten even more, then the point source assumption no longer holds and phase error corrections fail to improve the received power. The complex-conjugate method provides the actual correction needed at any distance.

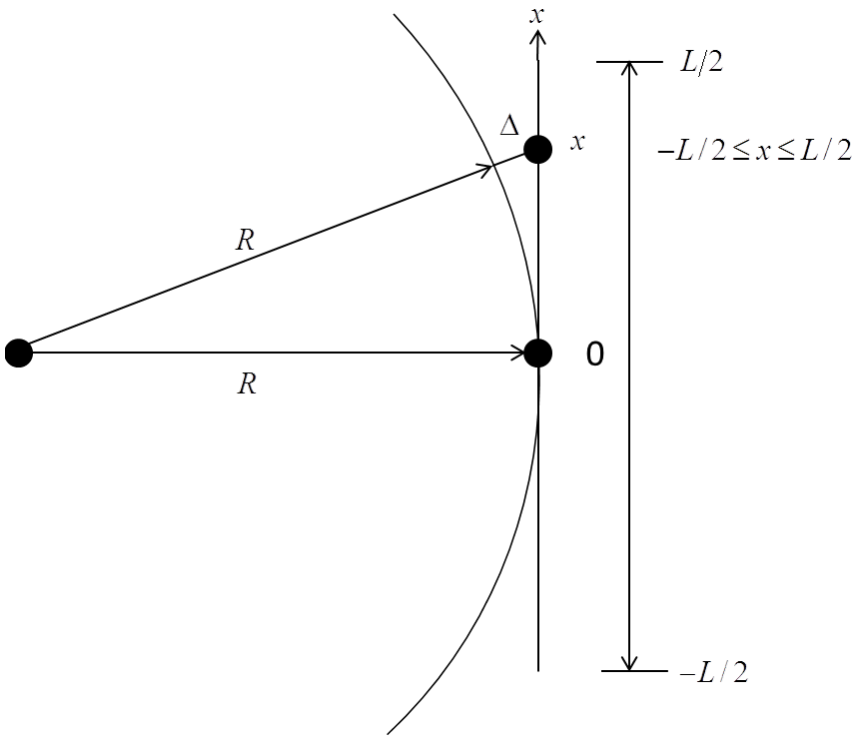

Figure 6. Path Length Difference for a Point Source Illuminating an Aperture

4. Conjugate-Matched Correction

In [27], it was shown that a complex conjugate match of the incident focused field resulted in an increased power transfer between antennas. Referring to Figure 5, we consider a receiver element (p,q) at distance y_{po}. The transmitter array has excitation coefficients G_{mn}, and the receiver array has coefficients A_{pq}. The transmission coefficient between element (m,n) and (p,q) is

$$g_{mnpq} = \frac{\sqrt{A_t \sin\theta_{mnpq} A_r \sin\theta'_{mnpq}}}{r_{mnpq}\lambda} \tag{35}$$

where A_t and A_r are the effective areas of each arrays' elements. We desire the G_{mn} for the field that is conjugate matched at the receiver plane y_{po}:

$$G^*_{mn} = \sum_p \sum_q g_{mnpq} A^*_{pq} e^{-j\beta r_{mnpq}}. \tag{36}$$

We apply these weights to the transmitter antenna. Extra processing is required, and it is necessary to know the location of the receiver array elements relative to the transmitter array elements. The complex-conjugate match method provides the correction for a specified geometry (spacing between arrays, array parameters, frequency, etc.). As opposed to quadratic-phase correction, the conjugate method utilizes both amplitude and phase corrections.

THIS PAGE INTENTIONALLY LEFT BLANK

III. SIMULATION

A. INTRODUCTION

1. Parametric Study Approach

The main goal of this research is to increase the power received by the receiver array by correcting the phase of the transmitter array or by correcting both the phase and amplitude of the transmitter array. Part of the parametric study revolves around confirming the results from [2] by varying the distance between a ten-by-ten transmitter array and a single receiver dipole. Once this is accomplished, an array replaces the dipole at the receiver end.

With arrays at both the transmitter and receiver, we vary parameters to determine which configuration increases the power received. Since the process was automated (discussed below), the uniform, spherical-phase correction method, and conjugate-match method are plotted on the same graph. Distance is varied from zero meters to two meters since anything beyond two meters is considered in the far field for our frequencies of consideration.

The size of each of the arrays are parameters of consideration for the effect on the power reception. One of the array sizes is kept constant while the other array size is changed. For example, if the size of the transmitter array is varied, then the receiver array has a constant size. The transmitter array was varied to be both smaller and larger than the receiver array. In our research the arrays both were kept square for simplicity. Due to the limitation of the available PC, we only investigated arrays up to 30-by-30.

Finally, the frequency was adjusted for each of the scenarios discussed above. We focused our research primarily in the Industrial, Scientific, and Medical (ISM) bands and the X-band (specifically 2.4 GHz, 5.8 GHz, and 10 GHz). The ISM band encompasses most of the commercial applications, and the X-band range covers radar applications.

2. Savant

Savant is an antenna simulation software that takes into account the installation environment such as a tank, car, building, or other platform. It can predict the radiated field distributions in the environment surrounding an antenna, the far-field radiation and receive patterns of antennas, and the cosite coupling/isolation between antennas mounted on the same platform or two separate platforms.

Savant's simulation method is based on the shooting-and-bouncing ray (SBR) method. Savant's SBR is a combination of two methods: geometrical optics (GO) and physical optics (PO). GO describes the simple ray-tracing techniques that have traditionally been used in optics. In order to use GO, it is assumed that wavefronts are locally planar and waves are TEM [28].

PO describes the approximation of the current induced "using ray optics to estimate the field on a surface and integrating that field over said surface to calculate the transmitted and scattered field" [29]. The PO induced current is [30]

$$\vec{J}_s = \begin{cases} 2\hat{n}_s \times \vec{H}^i, & \text{lit region} \\ 0, & \text{shadow} \end{cases}, \tag{37}$$

where $\hat{n}_s$ is the normal to the surface. As shown in Figure 7, $\vec{H}^i$ is the magnetic field incident on the scatterer. Using the radiation integral with the PO induced current, we obtain the scattered field,

$$\vec{E}^s(\vec{r}) = \frac{j\beta\eta_0}{4\pi}\iint_s \hat{k}\times\hat{k}\times\left[2\hat{n}_s\times\vec{H}^i\right]\frac{e^{-j\beta|\vec{r}-\vec{r}'|}}{|\vec{r}-\vec{r}'|}dS\,. \tag{38}$$

The position vectors to the source point $\vec{r}'$ and observation point $\vec{r}$ are shown in Figure 7.

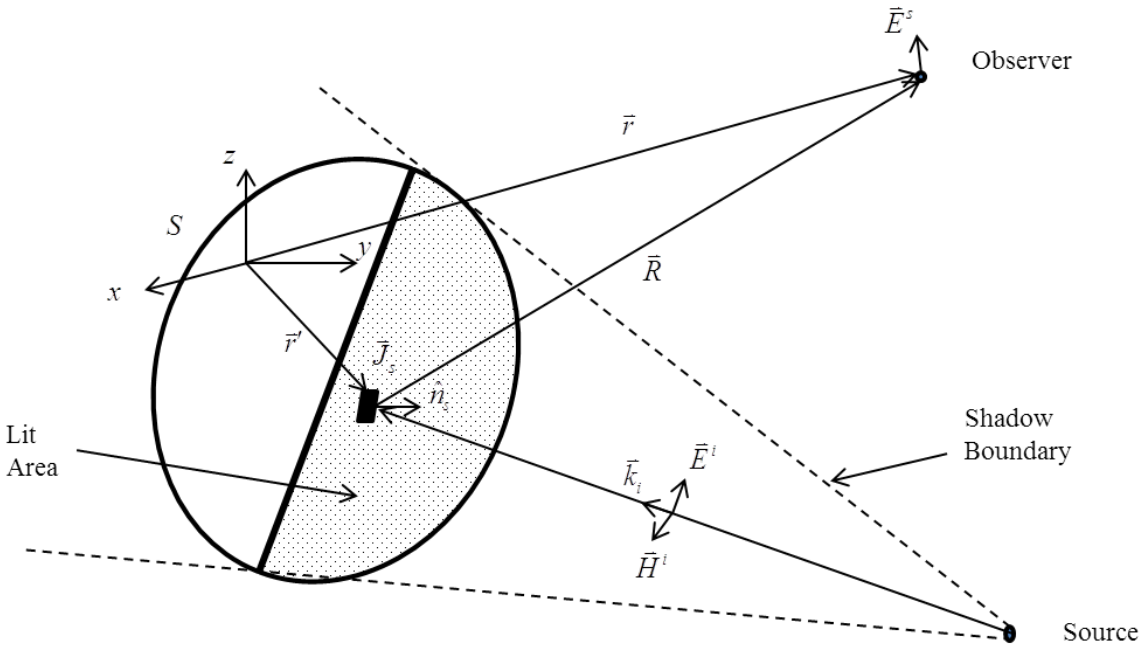

Figure 7. SBR Method for Determining the Scattered Electric Field

Savant launches the GO rays from the transmitter antenna towards the surface and determines which areas directly illuminated. The areas that are illuminated induce the PO currents that "radiate to far-field observation angles, near-field observation points, or receive antennas to generate scattered field contribution" [31]. These reflected GO rays travel and hit other surfaces in the installed environment, inducing secondary PO currents. As this process continues onto the next point and the next, Savant calculates multiple bounce scattering and determines the scattered fields for arbitrary shapes.

For antenna coupling, the expression

$$b = \frac{-j\lambda}{\sqrt{4\pi\eta_0}} \vec{E} \cdot \vec{d}_{Rx} \tag{39}$$

is used to determine the receive antenna's coupled power, where $\vec{d}_{Rx}$ is the scaled far-field directivity vector of the receive antenna, $\vec{E}$ is the incident or scattered electric field at the receiver antenna, and η_0 is the free-space impedance. The quantity b is the

complex amplitude of the received signal delivered to a transmission line that is impedance matched to the receive antenna.

Savant provides the user with easy to use functions. It accepts multiple computer-aided design (CAD) file formats, so whatever format used in the platform design can be accommodated and imported into Savant for simulation. Savant also comes with preloaded antenna shapes and sizes so a new user can run simulations on many common antennas. If the user has an antenna described in a Savant antenna element list (SARR) file, then Savant uses that file to generate its simulations. The three analysis types provide an easy to use interface for beginning the analysis. The user can create far-field patterns and field distributions ($\vec{E}$ and $\vec{H}$ fields) for installed transmit antennas. Coupling coefficients of the installed transmitter and receiver antennas can be derived. Once the analysis is completed, the color-coded visualization of the fields provides a tool for understanding where the power is distributed around the platform and environment.

Savant allows their application to be integrated into Matlab. The developers provided an application programming interface (API) for Matlab to run Savant via Matlab code. This functionality allowed for the parametric study to be automated. Savant also provided feedback on each run made, listing the details of its simulation.

Although Savant is relatively fast for analyzing antennas, the computational capability of a typical Windows desktop had a limit of 20-by-20 element arrays for the transmitter and receiver antennas. For a computer with a 3.4 GHz i7 Intel quad core processor and 24 GB of memory, each configuration can take up to six hours to complete, limiting the scope of the research. Because Savant uses SBR as its basis for analyzing antennas in their surroundings, the results are still an approximation of the real world. Other simulation techniques and measurements of the transmitter arrays and receiver arrays may not exactly match the results of these simulations.

3. Near Field vs. Far Field

In [2], Jenn presented the case that the focused array transmitter antenna to a single dipole receive antenna showed an improvement over the unfocused array

transmitter antenna. As part of this thesis we reaffirmed the results from [2] and present it in Figure 8. Although it is a simple case, the results shown in Figure 8 demonstrate the improvement possible using corrections. An operating frequency of 1 GHz was used for the simulation. The transmitter-array element spacing is half a wavelength apart and quarter of a wavelength above the ground plane. The receiver dipole antenna is half a wavelength long and is also a quarter of a wavelength above its ground plane. The scenario is depicted in Figure 9, with the transmitter array and dipole 1.0 m apart. As can be seen in Figure 8, the phase correction shows an improvement for the Fresnel field range. Within the 1.0 m range, the focused transmitter array delivers almost 15 dB more power to the receiver dipole as opposed to the unfocused array. Beyond 3.0 m there is no significant difference between the focused and unfocused array because the far-field conditions begin to take hold. Although the phase differences cause the focused and unfocused arrays to have different patterns, the radiation pattern shape in the far field is independent of distance. This case provides a good indicator for the improvement that can be achieved using a focused transmitter array.

From Figure 10, we present the more general Savant scenario of two arrays. The transmitter and receiver array elements are spaced is half a wavelength, and the elements are above the ground plane by a quarter of a wavelength. With Matlab automation discussed below, the operating frequency and distance between the transmitter and receiver array varies depending on the Matlab created Savant configuration file. The ground planes for both arrays extend a quarter of a wavelength beyond the array elements. The transmitter array elements have weights that are dependent on the SARR file. On the other hand, the receiver array elements use the default (uniform) weights from Savant.

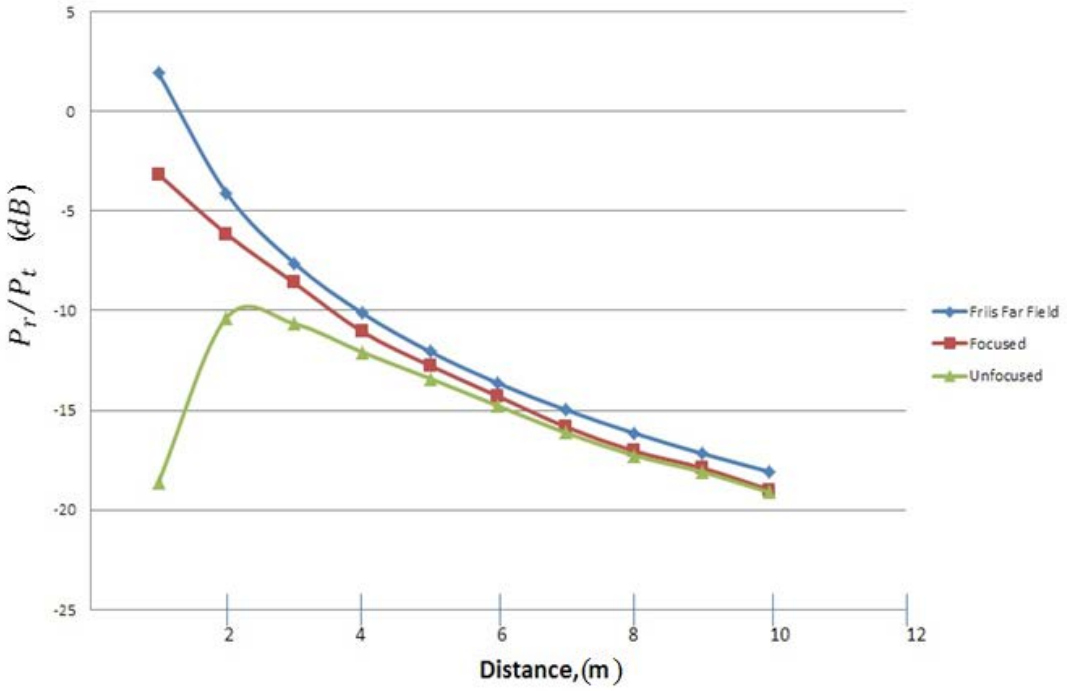

Figure 8. Coupling of a Ten-by-Ten Transmitter Array to a Single Dipole Receiver Antenna at 1 GHz

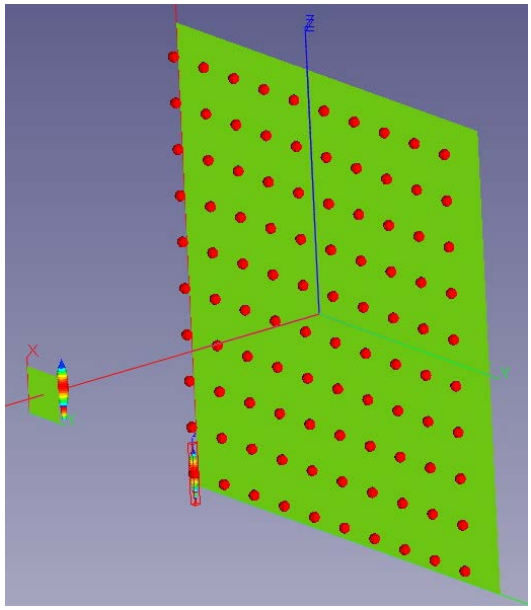

Figure 9. Savant Scenario of Ten-by-Ten Transmitter Array to Single Dipole at 1 GHz

The transmitter array takes advantage of Eqs. (3)–(5) and adjusts the phase from each element to the observation point along the *y*-axis in Figure 4. By doing this the transmitter array's main beam is focused at the dipole (as opposed to infinity for uniform phase) and a majority of the energy is incident on the receiver dipole.

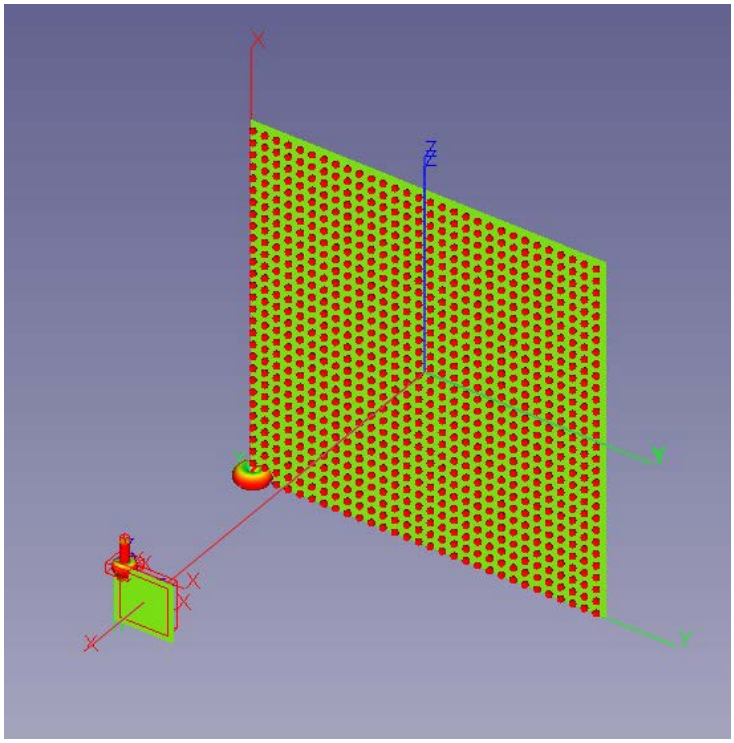

Figure 10. Savant Scenario of Transmitter Array Weighted SARR File and Receiver Array Using Default Savant Weights

4. Matlab Automation

In simulating a transmitter array to a single-dipole scenario, there was code to work with from [2]. The code creates the SARR files, which are Savant array element list files with weights of the transmitter array in the Savant scenario. The weights are determined by the frequency, number of elements, and distance between the transmitter array and the receiver array. With these parameters, the phase corrections are calculated and stored in the SARR file. For focusing using quadratic corrections, only phases are required. For conjugate corrections both amplitude and phase are required.

Savant allows the user to use preloaded antennas or antennas from file, so the transmitter array utilizes the "antenna from file" feature by loading the SARR file to represent the elements of the array. The receiver array consists of the preloaded rectangular array with a ground plane. Once loaded Savant creates the transmitter array from the SARR file and creates the receiver array from its library as shown in Figure 10 and Figure 11. Although Figure 9 and Figure 10 appear similar, the transmitter antenna is an array and a dipole, respectively. Also, the green plates are the ground planes for the two arrays and are set to be quarter of a wavelength behind the arrays. In Figure 11, the distance between the transmitter and receiver array configurations is 0.5 m and is shown for clarity. Savant also requires the type of antenna representation for each element of the array, so for this case, current sources were chosen for the dipole elements, and we only considered one reflection off the ground plane.

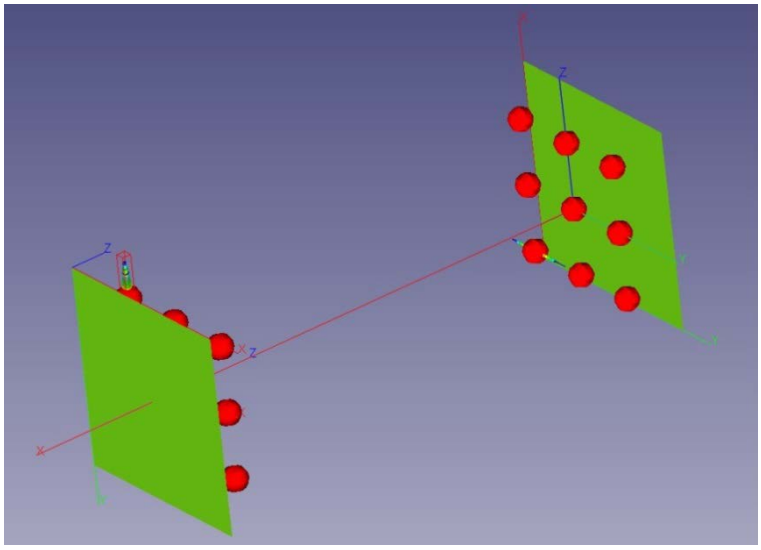

Figure 11. Savant Scenario of a Three-by-Three Transmitter Array to a Three-by-Three Receiver Array

The parameters were changed automatically to run each scenario. Parameters that must be changed include the distance, number of elements and frequency. For each case a new SARR file was created to focus the beam correctly; moreover, each change in array size demanded a change in the ground plate dimensions. This type of effort was required for both the unfocused transmitter array as well as the focused transmitter array.

Depending on the size of the arrays, each run required five to 30 minutes of computing time using the computer stated earlier for each datapoint. Automation saves time in running a large number of scenarios.

Savant's scenarios are stored in a configuration file based on extensible markup language (XML). XML is a markup language like the hypertext markup language (HTML) with an emphasis on storing and transporting data as opposed to displaying data. In the case of Savant, the configuration file contains tags for defining various aspects of the scenario such as antenna type, length of the array, frequency, etc. These different configuration tags are organized into nodes and tagged as "<NODE_CREATE>." For each antenna and ground plate node, there are dimension tags that exist to describe the length, width, and position of the array. In addition, the spacing between the elements of the array is modifiable. In order to change the SARR file, the text within the transmit array tag "<Filename>" was modified for the unfocused or focused SARR file. Lastly, to change the frequency, the data stored in the following tags were modified: <Frequency>, <ResonantFrequency>, "DesignFrequency>, <SingleFrequency>, and <MaxFrequency>. All modifications were done via Matlab since Matlab provides functions to create, modify, and delete XML files.

There are many parameters that can be adjusted to examine which method provides the best power reception. In this thesis the focus was on the frequency, distance between transmitter and receiver antennas, and the number of array elements. The spacing between elements in both arrays was kept to half a wavelength, so the frequency determined the spacing. This is an area that can be explored, but due to time limitations, we chose not to focus attention on spacing. Because of the limitations of processing power of the available computer, array sizes were kept below 30-by-30. As mentioned before, even with a 30-by-30 array, the Savant simulation took six hours to complete because of the increasing time to calculate bounces for every additional element. Additionally, the shapes of the arrays were restricted to a square configuration. We choose three different operating frequencies: 2.4 GHz, 5.8 GHz, and 10 GHz. The first two frequencies are based on the ISM band. ISM band consists of many common household items such as cellular signals, Bluetooth, and Wi-Fi. Air-to-air applications

such as radar warning receivers (RWR) and jammers commonly operate in the latter frequency band. Simulations were done by varying the distance between the arrays from 0.1 m to 2.0 m. These distances illustrated the effectiveness of the methods from near-field to far-field. Beyond 2.0 m, the far-field behavior exhibits inverse distance-squared behavior.

B. SIMULATION RESULTS

The results shown in this section are for several scenarios run on Savant using unfocused, focused, and complex-conjugate element excitations on the transmitter antenna.

1. Transmitter Array to Receiver Array

Since the receiver array is limited by the size of the UAV, the maximum number of elements is influenced by the choice of the frequency of operation. For small UAVs, typically the room allowed for the receiver array is about 6.0 inches; therefore, for 10 GHz, the largest receiver array size is about ten-by-ten elements. For the 5.8 GHz operating frequency, the largest array is six-by-six, and for the 2.4 GHz frequency, the largest array is two-by-two.

Two different methods are presented and compared to determine their effect on the power received. As was done with the single dipole receiver antenna, the quadratic-phase correction approach is the first method examined for its effectiveness. A further improvement on the focused approach is to take the complex conjugate of the field at the receiver element locations, thereby providing a complete match and delivering more power to the receiver array. The complex-conjugate method was proven very effective in [27]. The uniform method is used as a baseline to compare the effectiveness of the correction methods. As shown below, Figures 12 through 20 are plots of the antenna-to-antenna coupling P_r/P_t when $P_t = 1.0$ W. The case shown in Figure 12 verifies that all three excitations give the same result in the far field. For two-by-two arrays at 2.45 GHz, the far-field condition is satisfied at about $2D^2/\lambda = 2(0.0625)^2/0.125 = 0.0625$ m.

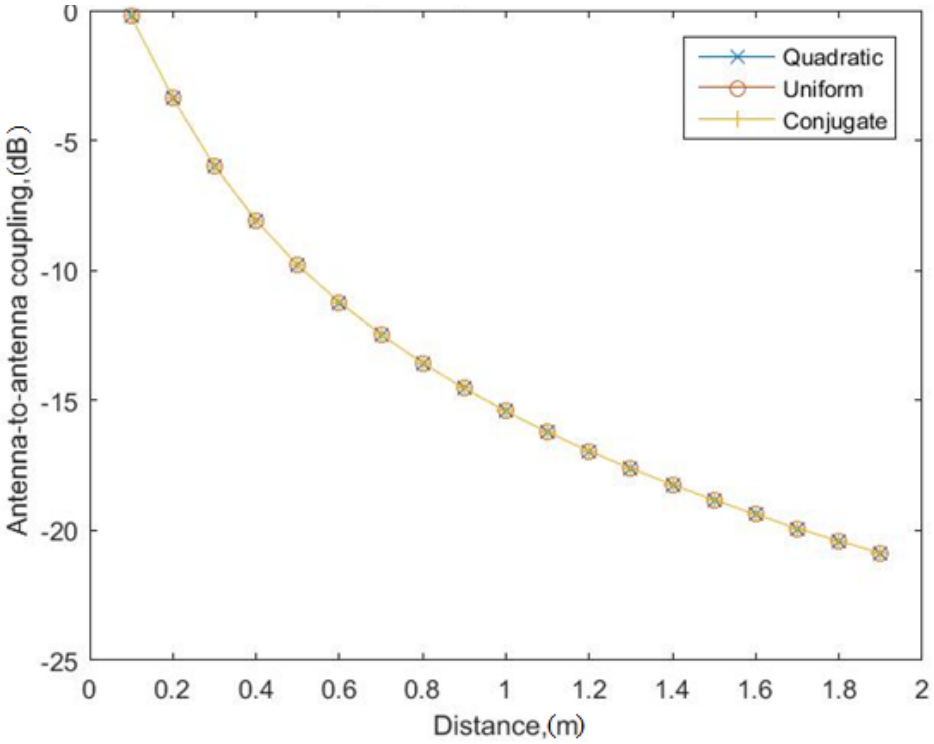

Figure 12. Power Received for a Transmitter Array (Two-by-Two) Excited by Uniform, Quadratic, and Conjugate Coefficients at a Receiver Array (Two-by-Two) at 2.4 GHz

2. Simulation of the Correction Methods

The focused spherical (quadratic) correction method requires only knowledge of the location of the center of the receiver array. This simplifies the processing and hardware at the transmitter array. Based on the study, the size of the transmitter array needs to be at least twice the size of the receiver array for the quadratic-correction method to be effective. As can be seen from Figures 13 and 14, the quadratic-phase correction method does not work well if the transmitter array is the same size or is smaller than the receiver array. From Figures 15 through 17, when the transmitter array dimensions are at least a factor of three greater than the receiver array, the power delivered at 0.5 m and more is increased by 3 dB or greater.

The quadratic-correction method does not work well when the distance between the transmitter array and receiver array is too small. The steep drop off in power received can be seen in Figures 13 through 17. From the receiver array observation point, the

transmitter array no longer looks like a point source, so the quadratic-phase correction method fails to improve the received power. The junction point can be seen where the power received in the uniform and quadratic-phase correction methods are equal in Figures 16 and 17. Once past this junction point, however, the quadratic-phase correction and conjugate-match method both improve the received power. As can be seen from Figure 16, from 1.4 m and on, both methods are equally better than uniform excitation.

The complex-conjugate method has the best results in regards to power delivered to the receiver array. The power delivered does not drop off when the distance between the transmitter array and the receiver array is too small. Even when the transmitter array's dimensions are equal or less than that of the receiver array, the conjugate-excited transmitter array maintains at least 0.5 dB advantage over the uniform method.

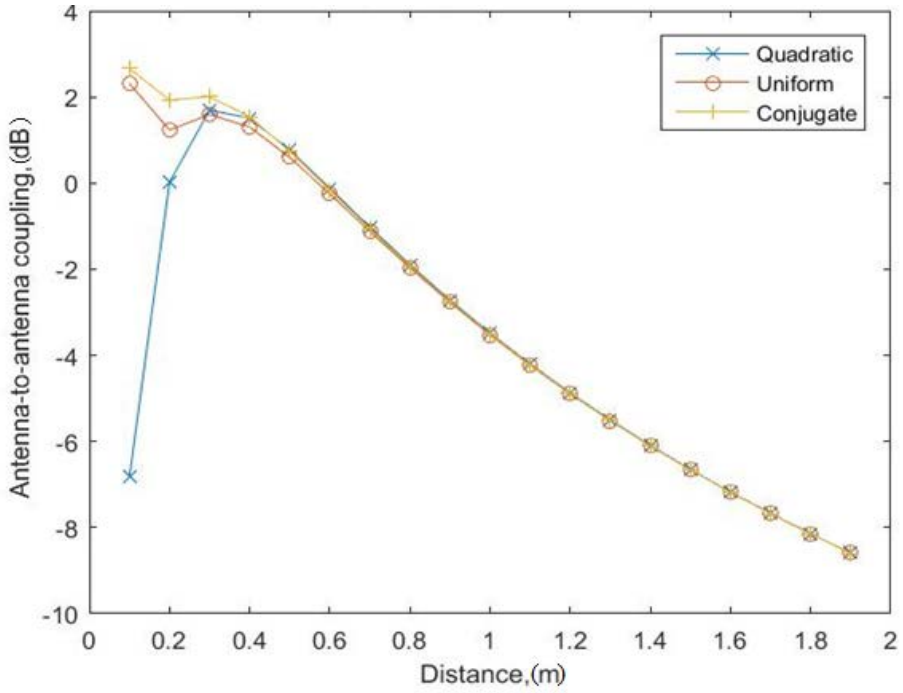

Figure 13. Power Received for a Transmitter Array (Six-by-Six) Excited by Uniform, Quadratic, and Conjugate Coefficients at a Receiver Array (Six-by-Six) at 5.8 GHz

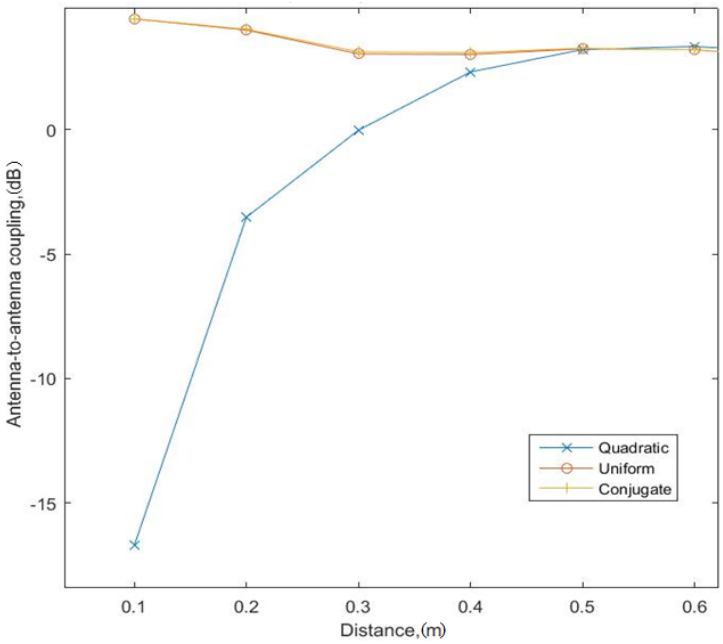

Figure 14. Power Received for a Transmitter Array (Ten-by-Ten) Excited by Uniform, Quadratic, and Conjugate Coefficients at a Receiver Array (Ten-by-Ten) at 10 GHz

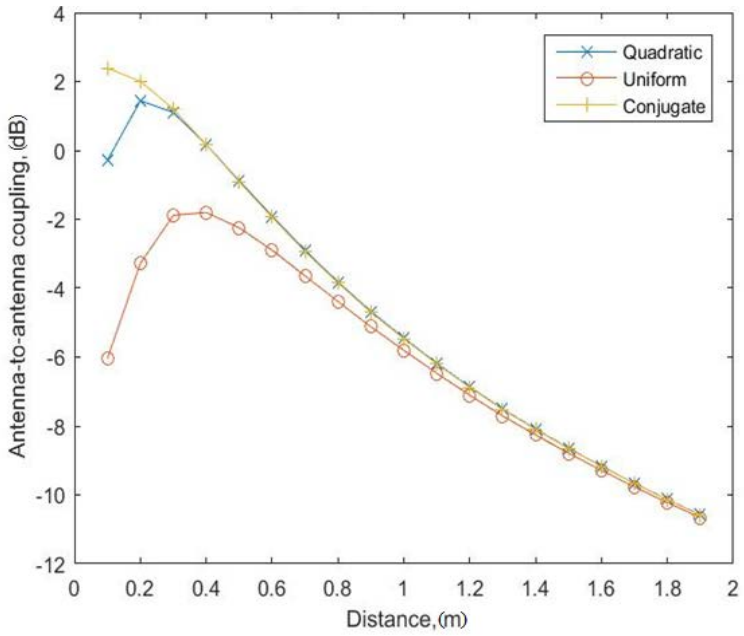

Figure 15. Power Received for a Transmitter Array (Six-by-Six) Excited by Uniform, Quadratic, and Conjugate Coefficients at a Receiver Array (Two-by-Two) at 2.4 GHz

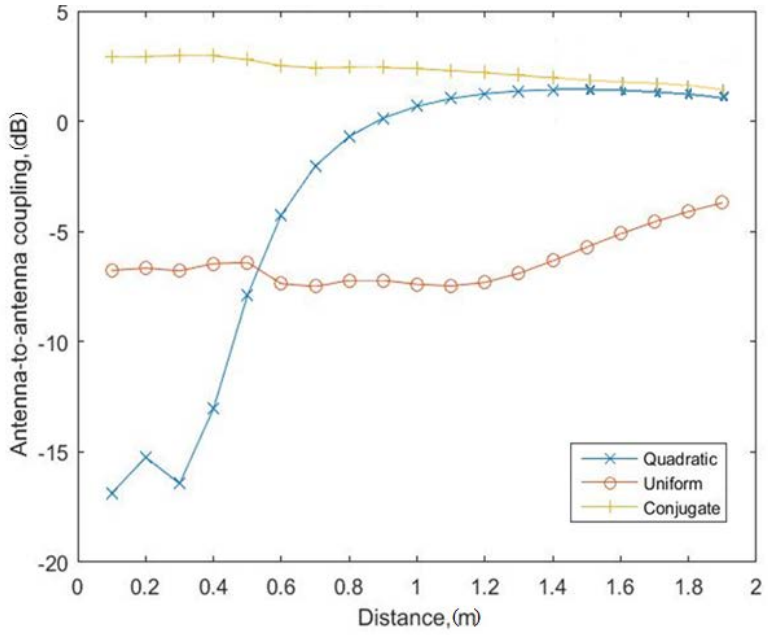

Figure 16. Power Received for a Transmitter Array (24-by-24) Excited by Uniform, Quadratic, and Conjugate Coefficients at a Receiver Array (Six-by-Six) at 5.8 GHz

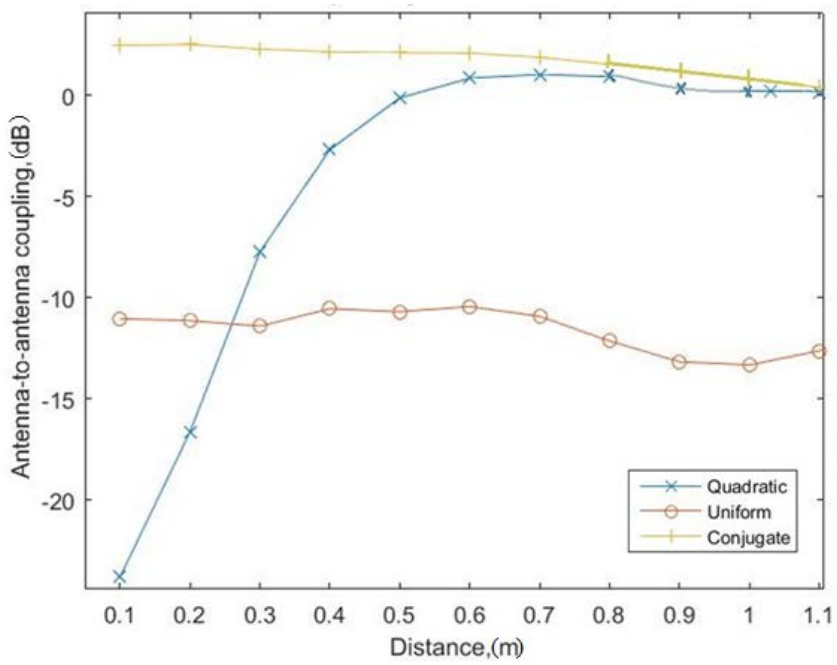

Figure 17. Power Received for a Transmitter Array (30-by-30) Excited by Uniform, Quadratic, and Conjugate Coefficients at a Receiver Array (Five-by-Five) at 10 GHz

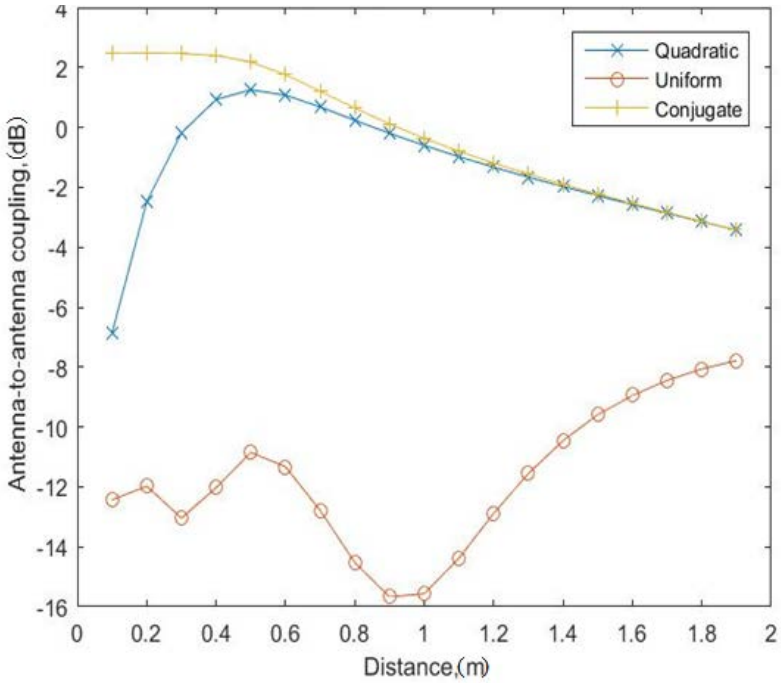

Figure 18. Power Received for a Transmitter Array (15-by-15) Excited by Uniform, Quadratic, and Conjugate Coefficients at a Receiver Array (Two-by-Two) at 2.4 GHz

The conjugate method requires knowledge of where all the elements are in both transmitter and receiver arrays. The extra processing power and hardware needed may not be worth the extra power delivered for distances less than 0.5 m; however, if the receiver array is stationary, then this only needs to be determined once and is up to the sponsors of the UAV program to decide. This is even more evident when we look at Figures 15 through 17. There is at least an 8.0 dB advantage over the uniform method for small distances.

The improvement in power over distance is proportional to the ratio of the transmitter array to the receiver array N_t/N_r, where N_t is the length of the transmitter array and N_r the length of the receiver array. For example, if we look at Figure 15 and Figure 18 at 1.0 m, the power received is –6 dB and –1 dB, respectively. If the UAV is 1.0 m away from the charging base station operating at 2.4 GHz, then we only need to design a 20-by-20 transmitter array using quadratic-phase correction. If the UAV requires charging at a much closer distance, such as 0.2 m, then we would design a four-by-four

transmitter array using quadratic-phase correction. The conjugate-match method provides the most versatile solution since the quadratic-phase correction method fails at close range when the transmitter array no longer looks like a point source. This research gives the designer guidelines to determine what method of correction is advantageous given their transmitter and receiver array sizes.

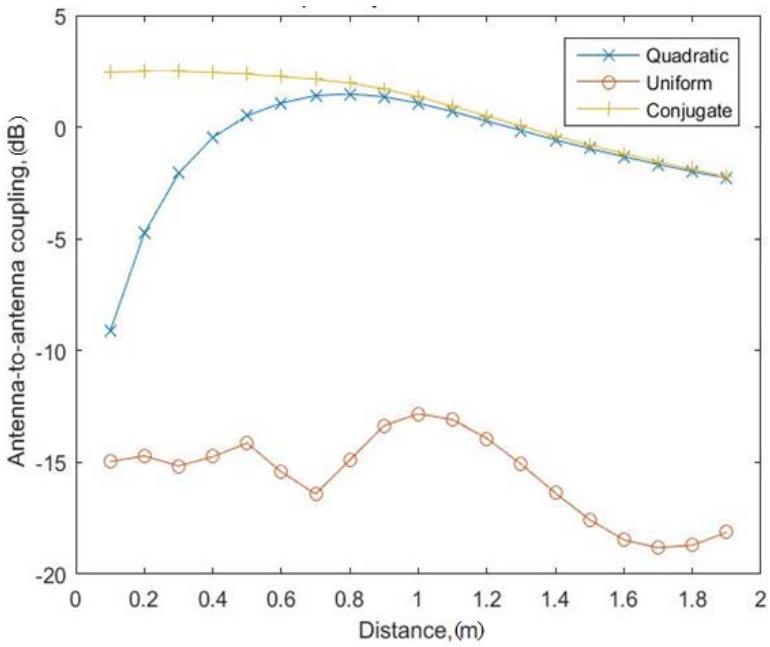

Figure 19. Power Received for a Transmitter Array (20-by-20) Excited by Uniform, Quadratic, and Conjugate Coefficients at a Receiver Array (Two-by-Two) at 2.4 GHz

3. Comparison of Analytical Formulas and Simulation

A simulation was performed to compare the analytical results obtained using Eq. (31) to simulated results. The data in Figure 20 compares the power received using the focused (quadratic correction) and unfocused cases. As can be seen in the near field range, the focused case provides an improvement over the uniform (unfocused) case. The curves fall in line with the behavior observed in the other simulations. As long as the transmitter array is seen as a point source, either focused methods may be used to improve power reception.

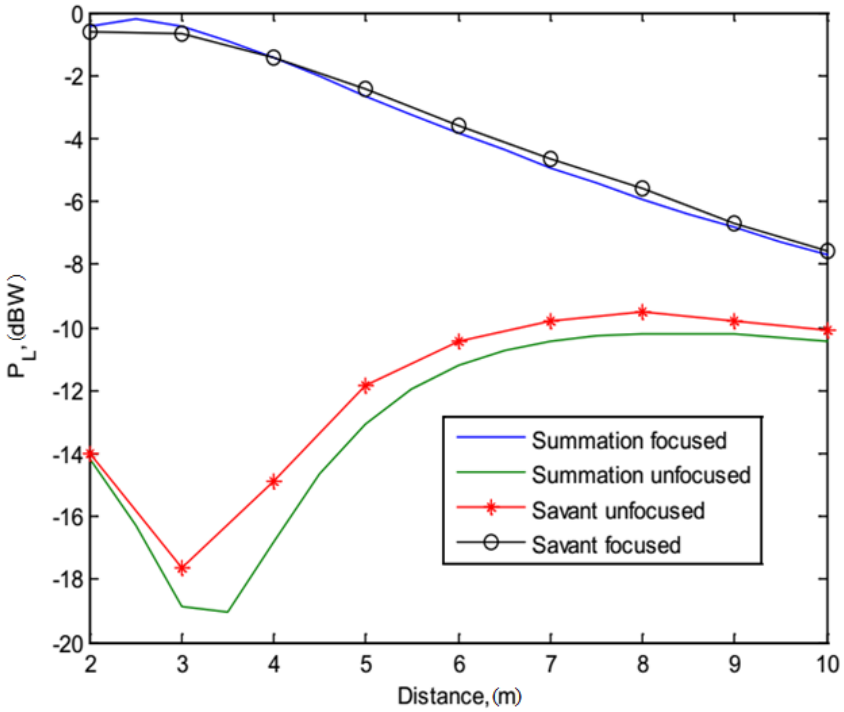

Figure 20. Power Received by a Single Dipole over a Ground Plane from a Ten-by-Ten Array with Ground Plane Transmitter 1 W at 300 MHz. Comparison of Summation Formula to Savant Simulations for Near-Field Ranges with and without Focusing. Source: [2].

THIS PAGE INTENTIONALLY LEFT BLANK

IV. CONCLUSIONS AND RECOMMENDATIONS

Our research is an extension of the technique proposed in [2] by considering two methods for correcting the phase errors between elements of the transmitter and receiver arrays in the near field. Using Savant and Matlab, we conducted a parametric study to determine which of the two methods increased the power received the most. By varying the sizes of the transmitter and receiver arrays, changing the frequency of operation, and varying the distance between the arrays, we discovered that the conjugate-match method consistently outperformed the spherical-phase correction method. Using the conjugate-match method, we found that the power received by the receiver array increased by as much as 12.0 Db, as long as there are a sufficient number of transmitter array elements as compared to receiver elements. Although the conjugate method is far superior to the spherical phase-correction method, it requires knowledge of the all the receiver element locations as well as calculation of the amplitude and phase weights. All these requirements mean more complex hardware and processing power.

If the receiver array is stationary, then the processor only needs to calculate the locations of the receiver elements once. Since the UAV is more likely than not stationary during charging, the conjugate-match method is a viable method for improved power transmission. With the ever increasing improvement in processing power, calculating a moving UAV array's receiver element locations may prove trivial enough that the conjugate-matching method can be used transfer power to a moving client.

Due to time constraints, several parameters were not investigated. In our scenarios, the transmitter and receiver arrays lined up center to center with no offset. This is an area that should be researched. Splitting the transmitter array into sub-arrays and focusing each sub-array on the center of the receiver array is the next step. As mentioned earlier, the spacing between the elements for the arrays was kept to a half a wavelength and exploring the effect of other spacings is worth pursuing. Changing the antenna type from a dipole is another study that could prove useful. Also, varying the length and width of the arrays rather than having square arrays might improve the power reception. A change in the CEM software is worth investigating. Full-wave solvers such as the method

of moments can include the mutual coupling between the array elements. The GO ray tracing does not rigorously model the mutual coupling between the arrays, which can be important at small distances. Also, cloud computing should be utilized to speed up the simulations.

APPENDIX

Consider element m,n to be a z-directed dipole at a height h above a ground plane that is located in the $x-z$ plane [2]. The ground plane factor is [2]

$$\begin{aligned} GPF &= e^{j\beta h\cos\alpha_{y_{mn}}} - e^{-j\beta h\cos\alpha_{y_{mn}}} \\ &= 2j\sin\left(\beta h\cos\alpha_{y_{mn}}\right) \end{aligned} \tag{40}$$

where $\cos\alpha_{y_{mn}} = v_{mn} = \sin\theta_{mn}\phi_{mn}$ is the direction cosine. The element factor for a z-dipole over the ground plane is [2]

$$\begin{aligned} EF_{mn} &= \hat{z}2j\sin\left(\beta h\sin\theta_{mn}\sin\phi_{mn}\right)\left(j60\frac{e^{-j\beta r_{mn}}}{r_{mn}}\frac{\cos\left(\frac{\pi}{2}\cos\theta_{mn}\right)}{\sin\theta_{mn}}\right) \\ &= -120\hat{z}\frac{e^{-j\beta r_{mn}}}{r_{mn}}\sin\left(\beta h v_{mn}\right)\frac{\cos\left(\frac{\pi}{2}w_{mn}\right)}{\sqrt{1-w_{mn}^2}}. \end{aligned} \tag{41}$$

The effective height is determined from

$$V_{mn} = \vec{E}\cdot\vec{h} \tag{42}$$

and

$$\vec{E}_{mn} = -j\eta\frac{I\beta}{4\pi r}e^{-j\beta r}\vec{h}_{mn}, \tag{43}$$

where $\vec{h}_{mn}$ is the effective height. For a half-wave dipole with a ground plane, the effective height is

$$\vec{h}_{mn} = -j\frac{4}{\beta}\frac{\cos\left(\frac{\pi}{2}\cos\theta_{mn}\right)}{\sin\theta_{mn}}\sin\left(\beta h\sin\theta_{mn}\sin\phi_{mn}\right)\hat{\theta}_{mn}\,. \tag{44}$$

Typically, we choose $h = \lambda/4$ so that $\beta h = \pi/2$. This is an idealized far-field result for an isolated element above an infinite ground plane. For a dipole in an array setting above a finite ground plane or in the near field, mutual coupling and diffraction affects the effective height and may not result in a $\sin\left(\beta h\sin\theta_{mn}\sin\phi_{mn}\right)$ factor. An efficiency factor *A* and taper exponent *B* can be added to the ground plane factor to characterize the behavior in the environment:

$$A\sin^{B}\sin\left(\beta h\sin\theta_{mn}\sin\phi_{mn}\right). \tag{45}$$

LIST OF REFERENCES

[1] M. Myers. (2015, April 16). SECNAV: F-35C Should be Navy's Last Manned Strike Jet. *Navy Times* [Online]. Available: http://www.navytimes.com/story/military/2015/04/16/navy-secretary-ray-mabus-joint-strike-fighter-f-35-unmanned/25832745/

[2] D. Jenn, "Short Range Wireless Power Transfer (WPT) for UAV/UAS Battery Charging - Phase I," Naval Postgraduate School, Monterey, CA, Tech. Rep. NPS-EC-14-004, Jan. 2014.

[3] I. Yoon and H. Ling, "Investigation of Near-Field Wireless Power Transfer in the Presence of Lossy Dielectric Materials," *IEEE Trans. Microw. Theory Tech.*, vol. 61, no. 1, pp. 482–488, Jan. 2013.

[4] H. Deng and L. Kong, "A Novel High-Efficiency Rectenna for 35 GHz Wireless Power Transmission," in *4th International Conf. on Microwave and Millimeter Wave Technology Proceedings*, Nanjing, China, Aug. 2004, pp. 114–117.

[5] Y. Peng, Z. Li and D. Qiao, "Prolonging Sensor Network Lifetime Through Wireless Charging," in *31st IEEE Real-Time Systems Symposium*, San Diego, CA, Dec. 2010, pp. 129–139.

[6] J. Ao, K. Takahashi, N. Shinohara, N. Niwa, T. Fujiwara and Y. Ohno, "S-parameter Analysis of GaN Schottky Diodes for Microwave Power Rectification," in *IEEE Compound Semiconductor Integrated Circuit Symposium*, Monterey, CA, Oct. 2010, pp. 1–4.

[7] D. Hambling. (2007, March). Power Up. *Defense Technology International* [Online]. 1(2). Available: http://www.nxtbook.com/nxtbooks/aw/dti0307index.php?startid=40

[8] R. Dickinson, "Power in the Sky: Requirements for microwave wireless power beamers for powering high-altitude platforms," *IEEE Microwave Magazine*, vol. 14, no. 2, pp. 36–47, Mar. 2013.

[9] Z. Popovic, "Cut the Cord: Low-Power Far-Field Wireless Powering," *IEEE Microwave Magazine*, vol. 14, no. 2, pp. 55–62, Mar. 2013.

[10] C. Balanis, *Antenna Theory, Analysis and Design*, 2nd ed. New York: John Wiley & Sons, 1997.

[11] W. Stutzman and G. Thiele, *Antenna Theory and Design*, 2nd ed. New York: John Wiley & Sons, 1998.

[12] W. C. Brown, “The history of power transmission by radio waves,” *IEEE Trans. Microw. Theory Tech*., vol. 32, no. 9, pp. 1230–1242, Sept. 1984.

[13] J. Zhang and C. Cheng, “Investigation of Near-Field Wireless Power Transfer Between Two Efficient Electrically Small Planar Antennas,” in *3rd Asia-Pacific Conference on Antennas and Propagation*, Harbin, China, July 2014, pp. 720–723.

[14] Y. Li and V. Jandhyala, “Design of Retrodirective Antenna Arrays for Short-Range Wireless Power Transmission,” *IEEE Transactions on Antenna and Propagation*, vol. 60, no. 1, pp. 206–211, Jan. 2012.

[15] Y. Kim, Y. J. Yoon, J. Shin and J. So, “X-band Printed Rectenna Design and Experiment for Wireless Power Transfer,” in *IEEE Wireless Power Transfer Conference*, Jeju, South Korea, May 2014, pp. 292–295.

[16] Q. Yuan, Q. Chen, J. Li and K. Sawaya, “Optimum Load of WPT System Analyzed by S-Parameters,” in *6th European Conference on Antennas and Propagation*, Prague, Czech Republic, March 2012, pp. 3604–3608.

[17] M. Dionigi, M. Mongiardo and S. Koziel, “Surrogate-Based Optimization of Efficient Resonant Wireless Power Transfer Links Using Conjugate Image Impedances,” in *44th European Microwave Conference*, Rome, Italy, Oct. 2014, pp. 429–432.

[18] J. Park, Y. Tak, Y. Kim, Y. Kim and S. Nam, “Investigation of Adaptive Matching Methods for Near-Field Wireless Power Transfer,” *IEEE Transactions on Antenna and Propagation*, vol. 59, no. 5, pp. 1769–1773, May 2011.

[19] N. Suksong, “Communications Antenna for a Micro RPV,” M.S. thesis, Dept. Elec. & Comp. Eng., Naval Postgraduate School, Monterey, CA, 1998.

[20] R. Vitale, “Design and Prototype Development of a Wireless Power Transmission System for a Micro Air Vehicle (MAV),” M.S. thesis, Dept. Elec. & Comp. Eng., Naval Postgraduate School, Monterey, CA, 1999.

[21] G. Tsolis, “Theoretical and Experimental Study of Micro Air Vehicle Powered by RF Signal at 10 GHz,” M.S. thesis, Dept. Elec. & Comp. Eng., Naval Postgraduate School, Monterey, CA, 2003.

[22] L. Tan, “Efficient Rectenna Design for Wireless Power Transmission for MAV Applications,” M.S. thesis, Dept. Elec. & Comp. Eng., Naval Postgraduate School, Monterey, CA, 2005.

[23] L. Toh, “A Follow-up Study on Wireless Power Transmission for Unmanned Air Vehicles,” M.S. thesis, Dept. Elec. & Comp. Eng., Naval Postgraduate School, Monterey, CA, 2007.

[24] C. Liu, “An Improved Rectenna for Wireless Power Transmission for Unmanned Air Vehicles,” M.S. thesis, Dept. Elec. & Comp. Eng., Naval Postgraduate School, Monterey, CA, 2011.

[25] C. Huang, “Design and Development of Wireless Power Transmission for Unmanned Air Vehiclees,” M.S. thesis, Dept. Elec. & Comp. Eng., Naval Postgraduate School, Monterey, CA, 2012.

[26] F. Ulaby, “Maxwell’s equations for time-varying fields,” in *Fundamentals of Applied Electromagnetics*, M. J. Horton, Ed. Upper Saddle River, NJ: Pearson Prentice Hall, pp. 255–270, 2007.

[27] N. S. Wong and R. Tang, “A Multielement High Power Monopulse Feed with Low Sidelobe and High Aperture Efficiency,” *IRE Transactions on Antennas and Propagation*, vol. 22, no. 3, pp. 402–407, May 1974.

[28] “Geometrical Optics and the Geometrical Theory of Diffraction,” class notes for Radiowave Propagation, Dept. Elec. & Comp. Eng., Naval Postgraduate School, Monterey, CA, Spring 2010.

[29] A. Kurasbek. (2015, Feb. 5). Geometrical Optics [Online]. Available: https://prezi.com/ebw8vhytvkgx/geometrical-optics/

[30] F. Vico, M. Ferrando, A. Valero, J. Herranz and E. Antonino. (2009). Computational Electromagnetics and Fast Physical Optics. Waves [Online]. 1(1). Available: http://www.iteam.upv.es/pdf_articles/81.pdf

[31] S. Sharma, “Shooting and Bouncing Analysis,” in *Handbook of Reflector Antennas and Feed Systems Volume I: Theory and Design of Reflectors*, Boston, MA: Artech House, 2013, pp. 31–32.

THIS PAGE INTENTIONALLY LEFT BLANK

INITIAL DISTRIBUTION LIST

1. Dudley Knox Library
   Naval Postgraduate School
   Monterey, California

2. Defense Technical Information Center
   Ft. Belvoir, Virginia